

Global Estimates of Wind Energy Input to Subinertial Motions in the Ekman-Stokes Layer

BIN LIU, KEJIAN WU and CHANGLONG GUAN*

Physical Oceanography Laboratory, Ocean University of China,
Qingdao, Shandong 266003, P.R. China

(Received 23 May 2006; in revised form 11 January 2007; accepted 15 January 2007)

By incorporating the wave-induced Coriolis-Stokes forcing into the classical Ekman model, the wind energy input to the Ekman-Stokes layer is investigated, with an emphasis on the surface wave effects when the direction of Stokes drift deviates from that of wind stress. Theoretical analysis of the kinetic energy balance of the Ekman-Stokes layer shows that the total wind energy input consists of the direct wind energy input and the wave-induced energy input. Details of the direct wind and wave-induced energy input are discussed. Based on the ECMWF ERA-40 Re-Analysis wind stress and surface wave data, the global total wind energy input to subinertial motions in the Ekman-Stokes layer is estimated at 2.19 TW, including 0.26 TW (12%) wave-induced energy input and 1.93 TW (88%) direct wind energy input. The effect of sea-ice coverage on the energy input to the Ekman-Stokes layer is also considered. It is shown that the global total energy input could be overestimated by 0.08 TW (about 4%) without taking the sea-ice coverage into account.

Keywords:

- Ekman-Stokes layer,
- Coriolis-Stokes forcing,
- wind energy input,
- subinertial motions,
- ERA-40.

1. Introduction

As winds blow over the sea surface, the wind stress at the air-sea interface will drag the ocean, which is associated with wind energy input to it. This wind energy input is an important component of the energetics of the global ocean, and has been investigated with a great deal of effort in the past. Faller (1966) first discussed the mechanical energy sources of ocean circulation, including wind stress, tidal dissipation and other sources. Lueck and Reid (1984) estimated that the total amount of energy flux to the ocean is about 2–10% of the downward energy flux (510 TW) in the atmospheric planetary boundary layer. Using satellite data and a numerical model, Wunsch (1998) estimated the wind energy input through the geostrophic current as 1.3 TW. Wind energy flux to near-inertial motions of the ageostrophic current is approximately 0.5–0.7 TW (Watanabe and Hibiya, 2002; Alford, 2003). Recently, Wang and Huang (2004a) employed the classical Ekman model to estimate global wind energy input to the subinertial motions of ageostrophic current as 2.3–2.4 TW. The wind energy flux to surface waves has also been estimated recently by Wang and Huang (2004b). However, in the studies mentioned above, the

wind energy inputs to currents and surface waves were investigated separately, and the effects of surface waves on the energy input to currents were not included.

As a ubiquitous phenomenon on the sea surface, a surface wave produces a mean Lagrangian flow, the so-called Stokes drift (Stokes, 1847), the direction of which is in accord with wave propagation. Hasselmann (1970) showed that the interaction between the planetary vorticity and the Stokes drift yields a Coriolis-Stokes forcing in the Eulerian momentum balance (see also Xu and Bowen, 1994; Sun *et al.*, 2004; Polton *et al.*, 2005). By incorporating this wave-induced Coriolis-Stokes forcing into the momentum balance of the Ekman layer (hereafter we refer to the Ekman layer with the effects of Stokes drift included as the Ekman-Stokes layer), Polton *et al.* (2005) pointed out that the Ekman-Stokes model agrees much more reasonably with the observational current profiles than the classical Ekman model. Similar results were also documented by Lewis and Belcher (2004).

Since the wave-induced Coriolis-Stokes forcing significantly modifies the current profile, it must somehow make contributions to the energy input to the ocean. More recently, Wu and Liu (2006, manuscript submitted to *J. Phys. Oceanogr.* in revision, hereinafter referred to as WL) have discussed the energetics of the Ekman-Stokes layer and found that energy input to the Ekman-Stokes layer comes from both the wind stress and the work done

* Corresponding author. E-mail: clguan@ouc.edu.cn

by the Coriolis-Stokes forcing. Using the NCEP/NCAR reanalysis wind stress data, WL estimated the energy input to subinertial motions in the Ekman-Stokes layer as 2.29 TW, 93% (2.14 TW) of which comes from direct wind energy input and 7% (0.15 TW) from wave-induced energy input. However, their estimates should be improved as they suffer from the following three limitations. First, they assumed that the direction of Stokes drift coincides with that of wind stress. However, this assumption does not hold in the real world ocean. The Stokes drift usually lies at an angle to the wind stress, especially for swell-dominant cases. Most recently, Chen *et al.* (2002) found that there are three “swell pools” in the oceans, based on wave climate analyses by satellite altimeter and scatterometer. Second, the Stokes drift was deduced from empirical formulas for fully-developed wind seas. Actually, surface waves in the ocean are mostly far from fully-developed, due to the time-varying wind or the limited fetch. Finally, high-latitude oceans are occasionally or permanently covered by sea ice. Intuitively, this sea-ice coverage could prevent the Ekman-Stokes layer from experiencing the action of the wind stress. Thus, the sea-ice coverage could also have an effect on the wind energy input to the Ekman-Stokes layer. Alford (2003) pointed out that the absence of sea-ice coverage would overestimate the wind energy input to ocean inertial motions at high latitude. Thus, a quantitative estimate of the effect of sea-ice coverage on the wind energy input to ocean current over the subinertial frequency is needed as well.

The present paper aims at estimating the wind energy input to subinertial motions in the Ekman-Stokes layer, using the European Centre for Medium-Range Weather Forecasts (ECMWF) ERA-40 Re-Analysis wind stress and surface wave data. We investigate the effect of the deviation of Stokes drift from wind stress on the wind energy input, and that of the sea-ice coverage. The paper is organized as follows: A brief introduction to the dynamics of the Ekman-Stokes layer and a detailed description of the wind energy input to the Ekman-Stokes layer are given in Section 2. Section 3 presents global estimates of energy input to subinertial motions in the Ekman-Stokes layer, and finally, some concluding remarks are given in Section 4.

2. Theory for Estimating Wind Energy Input to the Ekman-Stokes Layer

2.1 Momentum and kinetic energy balance of the Ekman-Stokes layer

Taking the wave-induced Coriolis-Stokes forcing into account, the horizontal momentum equation describing the unsteady state ageostrophic current in the Ekman-Stokes layer is expressed as (McWilliams *et al.*, 1997;

Lewis and Belcher, 2004; Polton *et al.*, 2005):

$$\frac{\partial \mathbf{U}}{\partial t} + f \hat{\mathbf{z}} \times (\mathbf{U} + \mathbf{U}_s) = \frac{\partial}{\partial z} \left(A_z \frac{\partial \mathbf{U}}{\partial z} \right), \quad (1)$$

where $\mathbf{U} = (u, v)$ is the horizontal current, A_z the vertical momentum diffusivity, t the time, z the vertical coordinate increasing upward from zero at the mean sea level, $\hat{\mathbf{z}}$ the unit vector directed upward, f the Coriolis parameter, and \mathbf{U}_s the Stokes drift, which, for deep water wave, is given by (Phillips, 1977):

$$\mathbf{U}_s = U_s e^{2kz} \hat{\mathbf{k}}, \quad U_s = a^2 \sigma k, \quad (2)$$

where a is wave amplitude, k wavenumber, $\hat{\mathbf{k}}$ the unit wavenumber vector, σ frequency, and U_s the velocity of Stokes drift at the sea surface. Note that the Stokes depth scale is $d_s = 1/(2k)$, with a typical value of 5–10 m. The boundary conditions are given as follows:

$$\rho_w A_z \frac{\partial \mathbf{U}}{\partial z} = \boldsymbol{\tau}, \quad \text{at } z=0; \quad \mathbf{U} \rightarrow 0, \quad \text{as } z \rightarrow -\infty, \quad (3)$$

where ρ_w is water density and $\boldsymbol{\tau}$ is sea surface wind stress.

Polton *et al.* (2005) gave the solution to Eq. (1) under the boundary conditions of Eq. (3) for a constant vertical diffusivity. Here, complex variable terms, namely the variables $\mathbf{U} = u + iv$, $\mathbf{U}_s = u_s + iv_s$, and $\boldsymbol{\tau} = \tau_x + i\tau_y$, are substituted for $\mathbf{U} = (u, v)$, $\mathbf{U}_s = (u_s, v_s)$ and $\boldsymbol{\tau} = (\tau_x, \tau_y)$ respectively, and the solution of Polton *et al.* (2005) can be expressed as:

$$\mathbf{U} = \mathbf{W}_e + \mathbf{W}_{es} + \mathbf{W}_s, \quad (4)$$

where

$$\mathbf{W}_e = \frac{\boldsymbol{\tau}}{\rho_w A_z j} e^{jz}, \quad \mathbf{W}_{es} = -\frac{2kj\mathbf{U}_s(0)}{(2k)^2 - j^2} e^{jz}, \quad \text{and}$$

$$\mathbf{W}_s = \frac{j^2 \mathbf{U}_s(0)}{(2k)^2 - j^2} e^{2kz}.$$

Here $j = (1 + i)/d$, $d = \sqrt{2A_z / f}$. The depth of the Ekman layer d_e , is defined as

$$d_e = \sqrt{\frac{2A_z}{|f|}}. \quad (5)$$

Note that Eq. (4) is applicable to both the Northern Hemisphere ($f > 0$, $d = d_e$) and the Southern Hemisphere ($f < 0$, $d = -d_e$).

0, $d = id_e$). The first term, \mathbf{W}_{es} , is purely the Ekman solution when the wave-induced effects are not taken into account. However, the second term, \mathbf{W}_{es} , and the third term, \mathbf{W}_s , are newly introduced due to the Coriolis-Stokes forcing. The Stokes component of the current \mathbf{W}_s , which is directly due to the Coriolis-Stokes forcing, decays within the Stokes depth scale d_s , while the Ekman-Stokes component of the current \mathbf{W}_{es} decays within the Ekman depth scale d_e . Thus the current profile in the Ekman layer could be modified by the Coriolis-Stokes forcing, and it is expected that the energy input to the Ekman layer could also be affected by the wave-induced Stokes drift.

Multiplying Eq. (1) by $\rho_w \mathbf{U}$ and integrating it from $z = -\infty$ to $z = 0$ gives the kinetic energy balance of the Ekman-Stokes layer:

$$\frac{dE}{dt} = E_w + E_s - D, \quad (6)$$

where

$$E = \rho_w \int_{-\infty}^0 \frac{1}{2} |\mathbf{U}|^2 dz, \quad E_w = \boldsymbol{\tau} \cdot \mathbf{U}(0),$$

$$E_s = \rho_w \int_{-\infty}^0 (-f \hat{\mathbf{z}} \times \mathbf{U}_s) \cdot \mathbf{U} dz, \quad \text{and} \quad D = \rho_w \int_{-\infty}^0 A_z \left| \frac{\partial \mathbf{U}}{\partial z} \right|^2 dz,$$

where E represents the total kinetic energy of the Ekman-Stokes layer, E_w the rate of direct wind energy input, E_s the rate of energy input caused by the interaction of Stokes drift with planetary vorticity, and D the dissipation rate. Apparently, the rate of energy input E_w is due to the work directly done by the wind stress. In contrast to the kinetic energy balance of the classical Ekman model (Wang and Huang, 2004a), E_s is a new energy input (hereinafter referred to as the wave-induced energy input) in the kinetic energy balance, which is due to the work done by the Coriolis-Stokes forcing per unit horizontal area of the water column. Considering that the Coriolis-Stokes forcing results from the wind-generated waves, E_s can be interpreted as the work done indirectly by the wind stress. For the steady-state case, the kinetic energy balance reduces to $E_w + E_s = D$, i.e., the total energy input, including the direct wind energy input E_w and the wave-induced energy input E_s , is balanced by the dissipation.

2.2 Wind energy input to the Ekman-Stokes layer

The direct wind energy input E_w and wave-induced energy input E_s can be rewritten as:

$$E_w = \text{Re}(\boldsymbol{\tau}^* \cdot \mathbf{U}(0)), \quad (7)$$

and

$$E_s = \rho_w f \int_{-\infty}^0 -\text{Im}(\mathbf{U} \cdot \mathbf{U}_s^*) dz, \quad (8)$$

where the symbol (*) denotes the complex conjugate, Re and Im denote the real and imaginary parts of a complex number, respectively.

Substituting Eqs. (2) and (4) into Eq. (7) yields:

$$E_w = E_{w,1} + E_{w,2} + E_{w,3}, \quad (9)$$

where

$$E_{w,1} = \frac{|\mathbf{d}|^2}{\rho_w d_e |f|}, \quad E_{w,2} = -\boldsymbol{\tau} \cdot \mathbf{U}_s(0) F_1(c), \quad \text{and}$$

$$E_{w,3} = \pm \hat{\mathbf{z}} \cdot (\boldsymbol{\tau} \times \mathbf{U}_s(0)) F_2(c) \begin{cases} +: f > 0 \\ -: f < 0 \end{cases}$$

where the non-dimensional Ekman-Stokes depth number c is defined as the ratio of the depth scale of the Ekman layer to that of the Stokes drift,

$$c = \frac{d_e}{d_s}, \quad (10)$$

and the expressions for $F_1(x)$ and $F_2(x)$ are

$$F_1(x) = \frac{x+2}{(x+1)^2+1}, \quad \text{and} \quad F_2(x) = \frac{x}{(x+1)^2+1}.$$

Note that the term $E_{w,3}$ is different for each hemisphere, taking “+” for the Northern Hemisphere ($f > 0$) and “-” for the Southern Hemisphere ($f < 0$). Equation (9) states that the direct wind energy input to the Ekman-Stokes layer consists of three terms. The first term, $E_{w,1}$, is exactly the wind energy input to the pure Ekman layer (Wang and Huang, 2004a). The second and the third terms, however, are new ones, because the surface current of the Ekman-Stokes layer is modified when the wave-induced Coriolis-Stokes forcing is taken into account. Both terms depend on wind stress, surface Stokes drift, the angle between the two vectors, and the Ekman-Stokes depth number.

Similarly, substitution of Eqs. (2) and (4) into Eq. (8) leads to:

$$E_s = E_{s,1} + E_{s,2} + E_{s,3}, \quad (11)$$

where

$$E_{s,1} = \rho_w |f| d_s |\mathbf{U}_s(0)|^2 F_3(c), \quad E_{s,2} = \boldsymbol{\tau} \cdot \mathbf{U}_s(0) F_1(c),$$

$$E_{s,3} = \pm \hat{\mathbf{z}} \cdot (\boldsymbol{\tau} \times \mathbf{U}_s(0)) F_2(c) \begin{pmatrix} +: f > 0 \\ -: f < 0 \end{pmatrix},$$

where $F_3(x)$ is

$$F_3(x) = \frac{x^2(x^3 - x^2 + 2)}{(x^4 + 4)[(x+1)^2 + 1]}.$$

Note that the wave-induced energy input to the Ekman-Stokes layer also consists of three terms. The first term depends on the magnitude of surface Stokes drift. The second term ($E_{s,2}$) is the same as that of the direct wind energy input, except of opposite sign, and it can be considered as part of the wind's work on the surface Stokes drift. The third term ($E_{s,3}$) is exactly the same as that of the direct wind energy input.

Based on the above expressions for the direct wind energy input and the wave-induced energy input, the total energy input to the Ekman-Stokes layer is obtained as:

$$\begin{aligned} E_{tot} &= E_w + E_s = E_{w,1} + E_{s,1} + 2E_{s,3} \\ &= \frac{|\mathbf{q}|^2}{\rho_w d_e |f|} + \rho_w |f| d_s |\mathbf{U}_s(0)|^2 F_3(c) \pm 2\hat{\mathbf{z}} \cdot (\boldsymbol{\tau} \times \mathbf{U}_s(0)) F_2(c) \\ &\quad \begin{pmatrix} +: f > 0 \\ -: f < 0 \end{pmatrix}. \end{aligned} \quad (12)$$

The total energy input includes the first term in direct wind energy input ($E_{w,1}$), the first term in wave-induced energy input ($E_{s,1}$), and the third terms in both direct wind and wave-induced energy inputs ($2E_{s,3}$). The second terms in both direct wind and wave-induced energy inputs make no contribution to the total energy input, as these two terms exchange energy between direct wind and wave-induced energy inputs via the Coriolis-Stokes forcing. Considering the limiting case $c \rightarrow \infty$, the depth of the Ekman layer is much greater than that of the Stokes drift layer, which corresponds to the case of small waves propagating over a very deep Ekman layer, $E_{w,2}$ or $E_{s,2}$ will tend to zero. For the limiting case $c \rightarrow 0$, the Ekman layer depth is much smaller than the Stokes drift depth, which corresponds to the case of large swells propagating over a very shallow Ekman layer, the value of $E_{w,2}$ or $E_{s,2}$ will reduce to $|\boldsymbol{\tau} \cdot \mathbf{U}_s(0)|$. Physically, under this limiting case the energy exchange between the two energy input paths is the work done by the wind stress directly on the sur-

face Stokes drift. As for the third terms in both direct wind and wave-induced energy inputs ($E_{w,3}$ and $E_{s,3}$), in both the limiting cases $c \rightarrow \infty$ and $c \rightarrow 0$, since $F_2(c) \rightarrow 0$, the their value tends to zero.

In contrast to the wind energy input to the pure Ekman layer ($E_{w,1}$), two additional terms are introduced into the energy input to the Ekman-Stokes layer. One is the first term in the wave-induced energy input ($E_{s,1}$), which always makes a positive contribution to the total energy input. The other is the term $2E_{s,3}$ (or $2E_{w,3}$) depending not only on the Coriolis parameter f but also on the angle between the wind stress and surface Stokes drift. For $f > 0$, if the Stokes drift lies to the left (right) of the wind stress, its contribution to the total energy input should be positive (negative). For $f < 0$, if the Stokes drift lies to the left (right) of the wind stress, its contribution should be negative (positive).

The above analyses are limited to the wind energy input to a steady Ekman-Stokes layer. However, in the real world ocean the motion in the Ekman-Stokes layer is far from the steady state, because of the time-varying wind forcing. The following is concerned with the energy input to the unsteady Ekman-Stokes layer.

Using the above-mentioned complex variables and their corresponding Fourier expansions

$$\mathbf{U} = \sum_{-\infty}^{\infty} \mathbf{U}_n e^{i\omega_n t}, \quad \mathbf{U}_s = \sum_{-\infty}^{\infty} \mathbf{X}_n e^{i\omega_n t}, \quad \text{and} \quad \boldsymbol{\tau} = \sum_{-\infty}^{\infty} \mathbf{T}_n e^{i\omega_n t},$$

the n -th component of horizontal momentum equation in the Ekman-Stokes layer can be written as:

$$i(f + \omega_n) \mathbf{U}_n + i f \mathbf{X}_n = A_z \frac{d^2 \mathbf{U}_n}{dz^2}. \quad (13)$$

The corresponding boundary conditions are:

$$\rho_w A_z \frac{\partial \mathbf{U}_n}{\partial z} = \mathbf{T}_n, \quad \text{at } z = 0; \quad \mathbf{U}_n \rightarrow 0, \quad \text{as } z \rightarrow -\infty.$$

Solving the above equation and substituting its solution into each energy input term of the corresponding kinetic energy balance equation, we can obtain the energy input for each component.

The direct wind energy input to the unsteady Ekman-Stokes layer for the n -th component is:

$$E_w^n = E_{w,1}^n + E_{w,2}^n + E_{w,3}^n, \quad (14)$$

where,

$$E_{w,1}^n = \frac{|\mathbf{T}_n|^2}{\rho_w d_e^n |f + \omega_n|}, \quad E_{w,2}^n = -\frac{f}{f + \omega_n} (\mathbf{T}_n \cdot \mathbf{X}_n(0)) F_1(c_n),$$

and

$$E_{w,3}^n = \pm \frac{f}{f + \omega_n} \hat{\mathbf{z}} \cdot (\mathbf{T}_n \times \mathbf{X}_n(0)) F_2(c_n) \begin{cases} +: f + \omega_n > 0 \\ -: f + \omega_n < 0 \end{cases}.$$

The wave-induced energy input for the n -th component can be expressed as:

$$E_s^n = E_{s,1}^n + E_{s,2}^n + E_{s,3}^n, \quad (15)$$

where

$$E_{s,1}^n = \rho_w \frac{f^2}{|f + \omega_n|} d_s^n |\mathbf{X}_n(0)|^2 F_3(c_n),$$

$$E_{s,2}^n = \frac{f}{f + \omega_n} (\mathbf{T}_n \cdot \mathbf{X}_n(0)) F_1(c_n),$$

and

$$E_{s,3}^n = \pm \frac{f}{f + \omega_n} \hat{\mathbf{z}} \cdot (\mathbf{T}_n \times \mathbf{X}_n(0)) F_2(c_n) \begin{cases} +: f + \omega_n > 0 \\ -: f + \omega_n < 0 \end{cases}.$$

Summing the energy inputs for each component, the total energy input to an unsteady Ekman-Stokes layer can be obtained as:

$$\begin{aligned} E_{tot} &= \sum_n (E_w^n + E_s^n) = \sum_n (E_{w,1}^n + E_{s,1}^n + 2E_{s,3}^n) \\ &= \sum_n \frac{|\mathbf{T}_n|^2}{\rho_w d_e^n |f + \omega_n|} + \sum_n \rho_w \frac{f^2}{|f + \omega_n|} d_s^n |\mathbf{X}_n(0)|^2 F_3(c_n) \\ &\quad \pm 2 \sum_n \frac{f}{f + \omega_n} \hat{\mathbf{z}} \cdot (\mathbf{T}_n \times \mathbf{X}_n(0)) F_2(c_n) \begin{cases} +: f + \omega_n > 0 \\ -: f + \omega_n < 0 \end{cases}. \end{aligned} \quad (16)$$

Note that d_e^n and c_n are defined for the n -th component as

$$d_e^n = \sqrt{\frac{2A_z}{|f + \omega_n|}} \quad \text{and} \quad c_n = \frac{d_e^n}{d_s^n} = \frac{d_e}{d_s} \sqrt{\frac{|f|}{|f + \omega_n|}}, \quad (17)$$

respectively, where d_s^n is the n -th component of the Stokes

depth scale d_s . The expressions of the energy input terms for the unsteady-state case are almost the same as those for the steady-state case, but taking the frequency ω_n of each component into account.

3. Global Estimates of the Energy Inputs

In previous studies (WL), the Stokes drift was computed from wind data only, with the empirical formulas applicable to fully-developed wind seas. In fact, the status of wind wave development in the ocean is variable and mostly far from fully-developed. For instance, the peak enhancement factor in the JONSWAP spectrum (Hasselmann *et al.*, 1973), a measure of the status of a wind wave, normally varies from 1.5 to 6, rather than unity, which corresponds to the fully-developed status. Thus, in the present paper, the ECMWF ERA-40 Re-Analysis wind stress and sea surface wind wave data are used to estimate the wind energy input to subinertial motions in the Ekman-Stokes layer, free of the limitation due to using the empirical formulas for fully-developed status. These datasets are regularly gridded with resolution 2.5° in both longitudinal and latitudinal directions, and cover the period from September 1957 to August 2002. Only the datasets from 1958 to 2001 are used, since the data in 1957 and 2002 are incomplete.

According to the above analysis, we first calculate the Stokes drift and its depth scale in order to estimate the wind energy input to the Ekman-Stokes layer. Substituting the deep water dispersion relation $\sigma^2 = gk$ into Eq. (2), and using the surface wave characteristics: significant wave height H_s , mean wave direction θ and mean wave period T , we have:

$$U_s = \frac{2\pi^3}{g} \frac{H_s^2}{T^3}, \quad \text{and} \quad d_s = \frac{gT^2}{8\pi^2}. \quad (18)$$

The Stokes drift is assumed to be in the same direction as the mean wave direction. It is difficult to compute the Ekman-layer depth directly from the vertical diffusivity, since there is no direct observation of the vertical diffusivity. The Ekman-layer depth is usually computed from an empirical formula $d_e = \gamma u_{*w}/f$, where u_{*w} is the friction velocity in water and γ is an empirical non-dimensional constant. The value of γ is commonly believed to be 0.25–0.5 (Coleman *et al.*, 1990; Cushman-Roisin, 1994; Price and Sundermeyer, 1999; Wang and Huang, 2004a). In the present study, following WL, we use the mean value ($\gamma = 0.38$) within the range of 0.25–0.5 to estimate the Ekman layer depth, i.e.:

$$d_e = 0.38 \frac{u_{*w}}{f}. \quad (19)$$

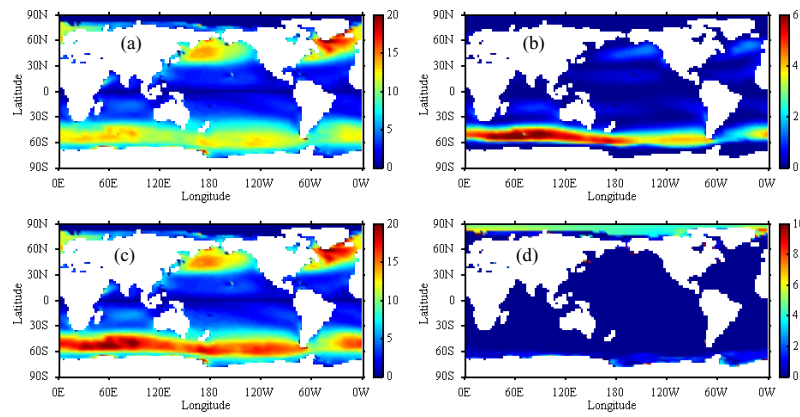


Fig. 1. Global distributions of (a) the direct wind energy input E_w , (b) the wave-induced energy input E_s , (c) the total energy input E_{tot} to the Ekman-Stokes layer, and (d) the difference of E_{tot} with and without the sea-ice coverage effects considered. Cutoff frequency is taken as $0.5 \text{ cycle day}^{-1}$ and unit is mW m^{-2} .

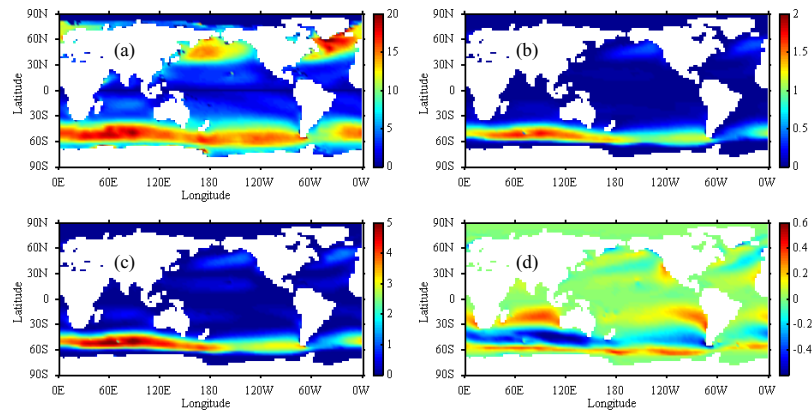


Fig. 2. Global distributions of (a) the first term in the direct wind energy input $E_{w,1}$, and the three terms including (b) $E_{s,1}$, (c) $E_{s,2}$ and (d) $E_{s,3}$ in the wave-induced energy input to the Ekman-Stokes layer (mW m^{-2}), with cutoff frequency at $0.5 \text{ cycle day}^{-1}$.

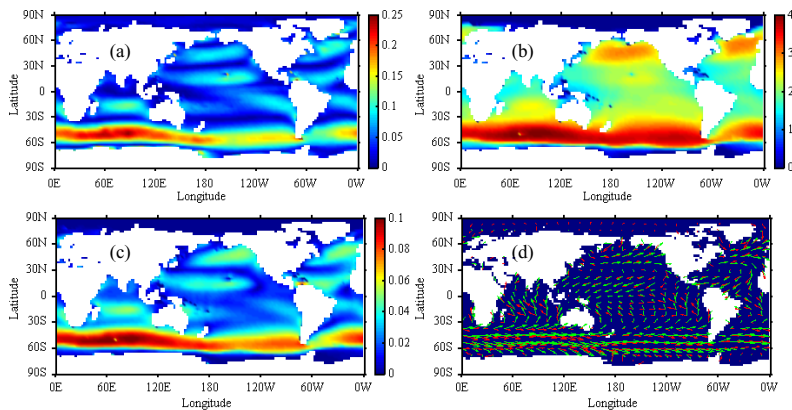


Fig. 3. Global distributions of the 44-year averaged wind stress (N), significant wave height (m), and surface Stokes drift (m s^{-1}). (a) Average wind stress. (b) Average significant wave height. (c) Averaged surface Stokes drift. (d) Directions of average wind stress (red arrows) and surface Stokes drift.

A time-averaged u_{*w} is used to compute the depth of the Ekman layer.

In order to estimate the global energy input to subinertial motions in the Ekman-Stokes layer, the components of the time series of wind stress $\boldsymbol{\tau}$, surface Stokes drift $\mathbf{U}_s(0)$ and its depth scale d_s are obtained at sea points with the complex-variable fast Fourier transform. Since the wind energy input to the Ekman-Stokes layer over the frequency of subinertial motions is considered in the present study, the cutoff frequency of ω is taken as $0.5 \text{ cycle day}^{-1}$. Note that the frequency $\omega < 0$ ($\omega > 0$) indicates clockwise (anticlockwise) rotating wind or Stokes drift component, and $\omega = 0$ corresponds to the steady component. Substituting these Fourier components into Eqs. (14)–(17), we can obtain the direct wind energy input, the wave-induced energy input and the total energy input for each Fourier component. The energy inputs at each grid point can then also be obtained.

Figures 1(a)–(c) show the global distributions of the direct wind energy input E_w , the wave-induced energy input E_s , and the total energy input E_{tot} to the Ekman-Stokes layer during 1958–2001, respectively. These distribution patterns are very similar to those presented in WL. The strong direct wind energy input and total energy input are found in the Antarctic Circumpolar Current (ACC) area and sub-polar basins in the North Pacific and North Atlantic Oceans, which correspond to the strong westerly wind belts in both hemispheres. However, the distribution patterns of the direct wind energy input and the total energy input are somewhat different. The maximum of the direct wind energy input is located over the North Atlantic Ocean, while that of the total energy input is located over the ACC area. The reason for this is that the wave-induced energy input to the Ekman-Stokes layer is mostly concentrated at the ACC area (see Fig. 1(b)), where the wave-induced energy input makes a significant contribution to the total energy input.

The global distributions of the first term in the direct wind energy input $E_{w,1}$, and the first, second and third terms in the wave-induced energy input to the Ekman-Stokes layer ($E_{s,1}$, $E_{s,2}$ and $E_{s,3}$) are shown in Figs. 2(a)–(d). The distribution pattern of the first term in direct wind energy input $E_{w,1}$ is quite similar to that of Wang and Huang (2004a, see Fig. 3). The distribution patterns of the first and second terms in the wave-induced energy input are similar to the pattern of the total wave-induced energy input, with strong energy input in the ACC area. Figure 3 shows the global distributions of the 44-year averaged wind stress, significant wave height and surface Stokes drift. It is demonstrated that within the ACC area both the mean wind stress and significant wave height are quite large, while the angles between the wind stress and surface Stokes drift are small. This is why the first and second terms in wave-induced energy input in this

area are much larger than those in other areas.

The distribution pattern of the third term $E_{s,3}$ in the wave-induced energy input (Fig. 2(d)) is different from those of the other two terms in the wave-induced energy input. It is clearly indicated that in the Southern Hemisphere the contribution of $E_{s,3}$ to the total energy input at the westerly wind belt is negative, while its contributions at both the trade-wind and polar easterly wind belts are positive. The feature of the distribution of $E_{s,3}$ in the Northern Hemisphere is similar to but not so clear as that in the Southern Hemisphere. The analyses in Subsection 2.2 indicate that the contribution of $E_{s,3}$ to the total energy input depends on the angle between the wind stress and the Stokes drift as well as the Coriolis parameter f . Figure 3(d) shows the directions of the averaged wind stress (red arrows) and Stokes drift (green arrows). In the westerly belt of the Southern Hemisphere ($f < 0$), the Stokes drift lies to the left of the wind stress, whereas on both sides of the westerly belt, the trade-wind belt and the polar easterly wind belt, the Stokes drift lies to the right of the wind stress. In the Northern Hemisphere ($f > 0$), the Stokes drift lies to the right of the wind stress in the westerly belt, and to the left of the wind stress in the trade-wind and polar easterly belts. The distribution of the angle between wind stress and Stokes drift could be related to the existence of swells. Based on wave climate analyses by satellite altimeter and scatterometer, Chen *et al.* (2002) found that there are three “swell pools”, corresponding to the trade wind regions in the three oceans (see their figure 7). The three “swell pools” also correspond to the areas where the Stokes drift deviates significantly from the wind stress. Large waves generated by strong winds in the westerlies propagate east- and equator-ward into the trade-wind belts, and east- and polar-ward into the polar eastlies. Since the winds in these two belts are usually westward, the average Stokes drift in these regions lies to the right of the average wind stress in the Southern Hemisphere, and to the left of the average wind stress in the Northern Hemisphere. The distribution of the angle between wind stress and Stokes drift results in the distribution pattern of the third terms ($E_{w,3}$ and $E_{s,3}$) of direct wind and wave-induced energy input. In addition, large positive contributions of $E_{w,3}$ and $E_{s,3}$ in the trade-wind belts are usually located in the eastern parts of the oceans, where the angles between wind stress and Stokes drift are large. The distributions of the total wave-induced energy input and its second term to the Ekman-Stokes layer also show a belt-like distribution, although not so clearly as that of $E_{s,3}$.

The wind energy input to the pure Ekman layer $E_{w,1}$, the direct wind energy input E_w , the wave-induced energy input E_s , and the total energy input E_{tot} to the Ekman-Stokes layer for the World Ocean are listed in Table 1 in detail. It is shown that in the Northern Hemisphere, the

component of energy input with $\omega < 0$ is larger than that with $\omega > 0$, while in the Southern Hemisphere the component of energy input with $\omega > 0$ is larger than that with $\omega < 0$. This means that the clockwise rotating components make greater contributions to energy input than the anticlockwise rotating components in the Northern Hemisphere; while in the Southern Hemisphere the anticlockwise rotating components are dominant. The estimated global total energy input to the Ekman-Stokes layer is 2.19 TW, including 0.26 TW wave-induced energy input (12% of the total amount) and 1.93 TW direct wind energy input (88% of the total amount).

Table 1 also shows that the wave-induced energy input is mostly caused by the steady component ($\omega = 0$) of wind stress and Stokes drift, which is mainly concen-

trated in the Southern Hemisphere, especially within the ACC (see also Fig. 1(b)), where the time-mean wind stress, significant wave height and surface Stokes drift are larger than those in other places (see Fig. 3). Compared with the amount of energy input to the pure Ekman layer (2.12 TW), the total amount of energy input only increases by 0.07 TW. The energy transferred between the direct wind energy input and the wave-induced energy input, however, can reach as much as 0.20 TW. Details of each component of wave-induced energy input are given in Table 2. It is shown that the steady component dominates the wave-induced energy input and the contributions from unsteady components are negligible.

Figure 4 shows the meridional distributions of the wind energy input to the pure Ekman layer ($E_{w,1}$), the direct wind energy input (E_w), the wave-induced energy input (E_s), and the total energy input (E_{tot}) by integrating the global energy distributions along latitudes. One dominant peak of these energy distributions lies between 35°S–60°S, and in the Northern Hemisphere there is also a sub-peak approximately between 35°N–60°N. The two peaks correspond to the westerly wind belts in both hemispheres. The major reason for the large difference between the two peaks in the westerlies of both hemispheres could be the much stronger wind stress in the ACC area in the Southern Hemisphere than that in the westerly belt of the Northern Hemisphere. The larger sea area in the ACC area in the Southern Hemisphere could also make significant contributions to this large difference. However, the strength of wind energy is the dominant factor in the total wind energy input to the Ekman-Stokes layer, since the wind energy input is proportional to the cube of wind speed, while it is linearly proportional to the sea area. It is illustrated that in the ACC area the wave-induced energy input makes a significant contribution to the total wind energy input, and that it is up to about 25% of the

Table 1. Distributions of the wind energy input to the pure Ekman layer ($E_{w,1}$), and the direct wind energy input E_w , the wave-induced energy input E_s , the total energy input E_{tot} to the Ekman-Stokes layer, with cutoff frequency at $\omega = 0.5$ cycle day⁻¹. All energy inputs in TW.

		$\omega > 0$	$\omega = 0$	$\omega < 0$	Sum
$E_{w,1}$	Northern Hemisphere	0.26	0.12	0.38	0.76
	Southern Hemisphere	0.61	0.36	0.39	1.36
	Total	0.87	0.48	0.77	2.12
E_w	Northern Hemisphere	0.26	0.09	0.38	0.73
	Southern Hemisphere	0.61	0.19	0.39	1.19
	Total	0.87	0.29	0.77	1.93
E_s	Northern Hemisphere	0.00	0.04	0.00	0.04
	Southern Hemisphere	0.00	0.22	0.00	0.22
	Total	0.00	0.26	0.00	0.26
E_{tot}	Northern Hemisphere	0.26	0.13	0.38	0.77
	Southern Hemisphere	0.61	0.42	0.39	1.42
	Total	0.87	0.54	0.77	2.19

Table 2. Distributions of each term ($E_{s,1}$, $E_{s,2}$ and $E_{s,3}$) in the wave-induced energy input (E_s) to the Ekman-Stokes layer, with cutoff frequency at $\omega = 0.5$ cycle day⁻¹. All energy inputs in GW.

		$\omega > 0$	$\omega = 0$	$\omega < 0$	Sum
$E_{s,1}$	Northern Hemisphere	0.02	7.14	0.00	7.16
	Southern Hemisphere	0.02	57.81	0.05	57.87
	Total	0.04	64.95	0.05	65.03
$E_{s,2}$	Northern Hemisphere	0.57	26.99	0.34	27.89
	Southern Hemisphere	0.50	167.11	0.45	168.06
	Total	1.07	194.10	0.79	195.95
$E_{s,3}$	Northern Hemisphere	-0.14	1.05	-0.01	0.91
	Southern Hemisphere	0.04	-1.62	-0.00	-1.58
	Total	-0.10	-0.57	-0.01	-0.68
E_s	Northern Hemisphere	0.44	35.18	0.33	35.95
	Southern Hemisphere	0.56	223.30	0.50	224.35
	Total	1.00	258.48	0.83	260.30

total energy input in some latitude belts.

As mentioned in Section 1, sea-ice coverage is capable of influencing the estimation of wind energy input to the World Ocean. In the present paper it is assumed that there is no wind energy flux to the ocean where the sea is covered by sea ice. Without the effect of sea-ice coverage, the total global energy input would reach as much as 2.27 TW (figure not shown), which is very close to WL's estimate (2.29 TW). This estimate for the total global energy input is overestimated by 0.08 TW in comparison with the present estimate with the effect of sea-ice coverage, which is 4% of the present estimate. Figure 1(d) shows the difference of E_{tot} with and without the effect of sea-ice coverage. The differences at the Arctic Ocean and the high latitude oceans near Antarctica are significant.

4. Conclusions

In the present paper, the wind energy input to the Ekman-Stokes layer is investigated by incorporating the wave-induced Coriolis-Stokes forcing into the classical Ekman model, with an emphasis on the surface wave effects when the Stokes drift is not in the same direction as the wind stress. As shown in Polton *et al.* (2005), the Coriolis-Stokes forcing plays an important role in determining the current profile of the Ekman-Stokes layer. The role of this wave-induced Coriolis-Stokes forcing in the energetics of the Ekman-Stokes layer is examined in the present paper.

Theoretical analysis of the kinetic energy balance of the Ekman-Stokes layer shows that the total wind energy

input consists of two parts, viz., the direct wind energy input and the wave-induced energy input. Both of them can be partitioned into three terms. The first term in the direct wind energy input is exactly the same as the wind energy input to the pure Ekman layer. The first term in the wave-induced energy input always makes a positive contribution to the total energy input. Both the second terms in direct wind and wave-induced energy inputs make no contribution to the total energy input, as they exchange energy within the Ekman-Stokes layer via the Coriolis-Stokes forcing. The second and the third terms, both in the direct wind energy input and in the wave-induced energy input, depend not only on the wind stress and the Stokes drift, but on the angle between them.

Using the ECMWF ERA-40 Re-Analysis wind stress and surface wave data, the total wind energy input to subinertial motions in the Ekman-Stokes layer for the World Ocean is estimated as 2.19 TW, including 0.26 TW wave-induced energy input (12% of the total amount) and 1.93 TW direct wind energy input (88% of the total amount). Neglecting the effect of sea-ice coverage would overestimate the total global energy by 0.08 TW (4% of the total amount). WL gives the total energy input as 2.29 TW, of which 93% (2.14 TW) refers to direct wind input and 7% (0.15 TW) to the wave-induced input. The difference in the total energy input between the two estimates is primarily due to the effect of sea-ice coverage, in addition to the effects of the angle between the Stokes drift and wind stress, and the growing wind wave status, and perhaps to the different wind datasets. In comparison with WL, it seems that the effect of the angle between the Stokes drift and wind stress, and the growing wind wave status increases the contribution of wave-induced input to the total energy input.

The contribution of the Coriolis-Stokes forcing to the total energy input seems marginal in terms of its energy input increase of 0.07 TW (3% of the total amount). However, the energy exchange due to the Coriolis-Stokes forcing between direct wind energy input and wave-induced energy input can reach as much as 0.20 TW (9% of the total amount).

The global distributions of energy input show that larger direct wind and total energy inputs appear at areas with strong wind and large surface waves, e.g. the westerlies in both hemispheres. The wave-induced energy input, which mainly comes from the contribution of steady components, is most significant within the ACC. Surprisingly, the third terms in wave-induced energy input and direct wind energy input make negative contributions to the total energy input in the westerly wind belts, but make positive contributions in the trade-wind belts and polar easterly wind belts in both hemispheres. This can be interpreted in terms of the global distribution of mean wind stress and surface waves, as well as the angle between

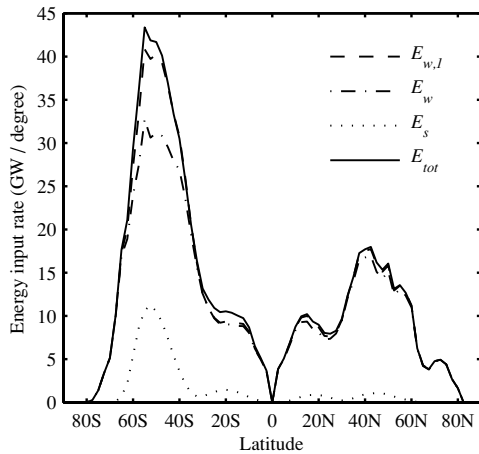


Fig. 4. Meridional distributions of wind energy input to the pure Ekman layer $E_{w,l}$ (dashed line), direct wind energy input E_w (dashdotted line), wave-induced energy input E_s (dotted line), and total energy input to the Ekman-Stokes layer E_{tot} (solid line), by integrating energy distributions along latitudes.

the wind stress and Stokes drift. The effect of sea-ice coverage on the energy input to the Ekman-Stokes layer is more significant in the Arctic Ocean and the high latitude oceans near Antarctica.

Acknowledgements

The authors appreciate support from the National Basic Research Program of China (Nos. 2005CB422302 and 2005CB422307) and also support from the National Natural Science Foundation of China (Nos. 40476008 and 40490263). The efforts to build the ERA-40 wind stress and surface wave data supplied by the ECMWF data server are really appreciated.

References

- Alford, M. H. (2003): Improved global maps and 54-year history of wind-work on ocean inertial motions. *Geophys. Res. Lett.*, **30**, 1424–1427.
- Chen, G., B. Chapron, R. Ezraty and D. Vandemark (2002): A global view of swell and wind sea climate in the ocean by satellite altimeter and scatterometer. *J. Atmos. Oceanic Technol.*, **19**(11), 1849–1859.
- Coleman, G. N., J. H. Ferziger and P. R. Spalart (1990): A numerical study of the turbulent Ekman layer. *J. Fluid Mech.*, **213**, 313–348.
- Cushman-Roisin, B. (1994): *Introduction to Geophysical Fluid Dynamics*. Prentice-Hall, Englewood Cliffs, New Jersey, 320 pp.
- Faller, A. J. (1966): Sources of energy for the ocean circulation and a theory of the mixed layer. *Proc. Fifth U.S. Congress of Applied Mechanics*, Minneapolis, Minnesota, ASME, p. 651–762.
- Hasselmann, K. (1970): Wave-driven inertial oscillations. *Geophys. Fluid Dyn.*, **1**, 463–502.
- Hasselmann, K., T. P. Barnett, E. Bouws *et al.* (1973): Measurements of wind-wave growth and swell decay during the Joint North Sea Wave Project (JONSWAP). *Deut. Hydr. Zeit.*, **A8**(12), 1–95.
- Lewis, D. M. and S. E. Belcher (2004): Time-dependent, coupled, Ekman boundary layer solutions incorporating Stokes drift. *Dyn. Atmos. Ocean.*, **37**, 313–351.
- Lueck, R. and R. Reid (1984): On the production and dissipation of mechanical energy in the ocean. *J. Geophys. Res.*, **89**, 3439–3445.
- McWilliams, J. C., P. P. Sullivan and C. H. Moeng (1997): Langmuir turbulence in the ocean. *J. Fluid Mech.*, **334**, 1–30.
- Phillips, O. M. (1977): *Dynamics of the Upper Ocean*. Cambridge Univ. Press, Cambridge, 336 pp.
- Polton, J. A., D. M. Lewis and S. E. Belcher (2005): The role of wave-induced Coriolis-Stokes forcing on the wind-driven mixed layer. *J. Phys. Oceanogr.*, **35**, 444–457.
- Price, J. F. and M. A. Sundermeyer (1999): Stratified Ekman layers. *J. Geophys. Res.*, **104**, 20467–20494.
- Stokes, G. G. (1847): On the theory of oscillatory waves. *Trans. Camb. Phil. Soc.*, **8**, 441–455.
- Sun, F., S. Gao, W. Wang and C. C. Qian (2004): Wave-induced stress and estimation of its driven effect on currents. *Science in China, Ser. D*, **47**, 1147–1154.
- Wang, W. and R. X. Huang (2004a): Wind energy input to the Ekman layer. *J. Phys. Oceanogr.*, **34**, 1267–1275.
- Wang, W. and R. X. Huang (2004b): Wind energy input to the surface waves. *J. Phys. Oceanogr.*, **34**, 1276–1280.
- Watanabe, M. and T. Hibiya (2002): Global estimates of the wind-induced energy flux to inertial motions in the surface mixed layer. *Geophys. Res. Lett.*, **29**, 1239–1242.
- Wunsch, C. (1998): The work done by the wind on the oceanic general circulation. *J. Phys. Oceanogr.*, **28**, 2332–2340.
- Xu, Z. G. and A. J. Bowen (1994): Wave- and wind-driven flow in water of finite depth. *J. Phys. Oceanogr.*, **24**, 1850–1866.